Received: 4 March 2024 | Revised: 20 July 2024 | Accepted: 20 August 2024

DOI: 10.1002/mop.34317

RESEARCH ARTICLE

WILEY

A novel UWB in-body printed microstrip feed monopole antenna with dual band-stop capabilities

Mousa Abdollahvand[1] | **Yashar Zehforoosh**[2] | **Banafsheh Marufi**[2] | **P. Esmailzadeh Kaleybar**[2] | **Aliakbar Dastranj**[3]

[1]Department of Electrical and Computer Engineering, University of Mohaghegh Ardabili, Ardabil, Iran

[2]Department of Electrical and Engineering, Urmia branch, Islamic Azad University, Urmia, Iran

[3]Electrical Engineering Department, Faculty of Engineering, Yasouj University, Yasouj, Iran

Correspondence
Mousa Abdollahvand, Department of Electrical and Computer Engineering, University of Mohaghegh Ardabili, Ardabil, Iran.
Email: m.abdollahvand@uma.ac.ir

Abstract

This paper presents an innovative and condensed blueprint for an ultra-wideband (UWB) printed monopole antenna, aiming to augment bandwidth and achieve dual band-stop capabilities, all while accounting for the impact of the human body model on stop bands. The proposed design showcases a square radiating patch situated on the top layer of the substrate, complemented by a ground plane etched on the underside, integrating two sets of adapted U-shaped slots. Such a configuration delivers a broad operational fractional bandwidth that surpasses 132%. Within our design, a modified C-shaped slot in the radiation patch creates the first band-stop property, while a pair of modified F-shaped slots etched in the radiation patch generates the second stop-band property. Measuring 12 mm × 18 mm × 0.8 mm, the antenna offers a compact form factor, broad bandwidth, cost-effectiveness, omnidirectional radiation patterns within the H-plane and acceptable behavior for using in In-body microwave applications.

KEYWORDS

dual band-stop capabilities, in-body printed monopole antenna, omni-directional radiation patterns, ultra-wideband (UWB) system

1 | INTRODUCTION

The Federal Communications Commission (FCC) regulates ultra-wideband (UWB) frequencies spanning from 3.1 to 10.6 GHz.[1] In UWB monopole antennas, a major challenge is designing a highly compact printed monopole antenna that achieves wideband performance across the entire operating frequency band while maintaining omnidirectional radiation patterns in the H-plane.[2] One proposed solution for UWB applications is a double-fed printed monopole antenna with a truncated ground plane and a radiating patch featuring a dual annular structure.[3] However, these UWB antennas are prone to interference from various narrow-band systems, such as C-band (4–8 GHz), WiMAX (3.3–3.7 GHz), WLAN (5.15–5.35 GHz), and X-band downlink satellite communication frequencies, due to overlapping bandwidths. Although there are reports of UWB antennas with single band-stop functions, performance within the UWB spectrum can be improved by incorporating dual band-stop functions.[4-7] In this design, we aim to reject two specific frequency bands within the UWB range (3.1–10.6 GHz): WiMAX (3.3–3.7 GHz), and WLAN (5.15–5.825 GHz).

Wireless body area networks (WBANs) have diverse applications in healthcare, public safety, and defense, enabling monitoring and communication. WBAN systems are typically classified into wearable and implantable categories. Wearable systems are positioned on the human body, while implantable systems are embedded within human tissues. Wearable systems can be further classified into on-body, in-body, and off-body communication links.

This study specifically focuses on in-body wearable systems.[8]

Breast cancer is a significant global health concern, driving the need for antennas suitable for integration into microwave imaging systems. Challenges include antenna size, gain, radiation efficiency, and narrow impedance bandwidth.[9,10] Several wideband antennas have been designed for microwave medical imaging systems, but printed monopole antennas are a particularly popular choice for this application. This is due to their ability to operate over a wide frequency range with minimal structural modifications and a compact footprint.[11,12] On the other hand, to ensure the safety of the human body and determine its exposure to radio waves, the Specific Absorption Rate (SAR) is commonly used in wireless devices. For this purpose, you must adhere to the regulatory guidelines on SAR.[13] To minimize SAR levels and comply with the FCC standard (maximum of 1.6 W/kg averaged over 1 g of tissue) or the ICNIRP standard (maximum of 2 W/kg averaged over 10 g of tissue), several techniques have been implemented.[11,13] Therefore, there is a need for an innovative, compact UWB printed antenna featuring dual-band-stop capabilities, which holds particular promise for breast cancer detection.

Several techniques have been suggested to incorporate band-stop characteristics into antennas, including the integration of stubs within the patch and the utilization of a G-shaped slot-defected ground structure (DGS).[6] Other techniques include four crescent-shaped nested rings,[14] using the Iron shaped parasitic resonators and inverted U-shaped,[15] combining a slot and mushroom-shaped electromagnetic-bandgap,[16] placing inverted U-shaped strip close to the microstrip feed line and positioning an inverted U-shaped slot on the radiating surface,[17] incorporating L-shaped stubs into the notched patch,[18] a conductor-shaped resonator and an inverted U-shaped resonator on a partial ground plane,[19] altering the upper layer of the antenna with protruding L-shaped strips inside the square radiation stub and a protruding E-shaped strip inside the feed line,[20] are another approach to achieving band-stop features in antennas. These methods aim to introduce a dual band-stop characteristic to reject interference in UWB antennas.

In our study, we developed a UWB antenna to enhance bandwidth for in-body microwave imaging applications.[8] Our focus was on improving bandwidth by introducing a novel dual band-stop monopole antenna. Additionally, we investigate how the human body model affects frequency band-stop properties. Our findings suggest that our proposed dual-band-stop antenna is suitable for microwave imaging systems and free space, especially when isolated from the human body.

This paper introduces a novel monopole antenna with dual-band-stop capabilities and an extended bandwidth with acceptable behavior for using in in-body microwave applications. Unlike existing dual band-stop UWB antennas, our proposed design offers a simplified structure, leading to reduced fabrication costs. Additionally, it maintains monopole-like patterns with adequate gain and radiation efficiency across the frequency spectrum. Our design achieves a significantly wider impedance bandwidth by integrating two pairs of straightforward and modified U-shaped slots on the back layer. Additionally, the introduction of a novel modified C-shaped slot within the radiation patch enhances the initial band-stop feature, thus further improving the impedance bandwidth. The dual band-stop characteristic is achieved through the inclusion of a pair of slots with modified F-shapes in the radiation patch. Remarkably, our proposed antenna distinguishes itself with its compact size compared to other referenced dual band-stop UWB antennas, meanwhile, it maintains a broad impedance bandwidth ranging from 2.9 to 14.2 GHz, while featuring two stop-bands at 3.3–4.2 and 5.2–5.8 GHz and suitable SAR values for using in in-body microwave imagine applications.

2 | ANTENNA DESIGN AND DIMENSIONS

Figure 1 displays the layout of our extended dual-band-stop antenna design. As shown, our antenna design includes a radiating patch with a pair of modified F-shaped slots, a modified C-shaped slot, and two pairs of modified inverted U-shaped slots on the back layer. The designed patch is connected to a microstrip feed line. The ground plane, defined by dimensions W_{sub} and L_{gnd}.

In the preliminary stages of designing our proposed structure, we assign specific values to the antenna dimensions. Our suggested monopole antenna is constructed on an economical FR4 substrate with a relative permittivity of 4.4, measuring 12×18 mm^2 in dimension and 0.8 mm in thickness. To attain the desired characteristic impedance of 50 Ohms in the designed feed line, W_f is established at 1.5 mm. Additionally, initial values for W and L are chosen to determine the dimensions of the designed radiating patch, as outlined below:

$$W = \frac{v_0}{2f_{center}}\sqrt{\frac{2}{\varepsilon_r + 1}}, L = \lambda_{lower}/4, \quad (1)$$

where λ_{lower} and f_{center} are the lower bandwidth wavelength and center of operating frequencies, respectively. The parameter W plays a crucial role in determining the antenna's bandwidth. As this parameter increases, the antenna's bandwidth expands accordingly, whereas it

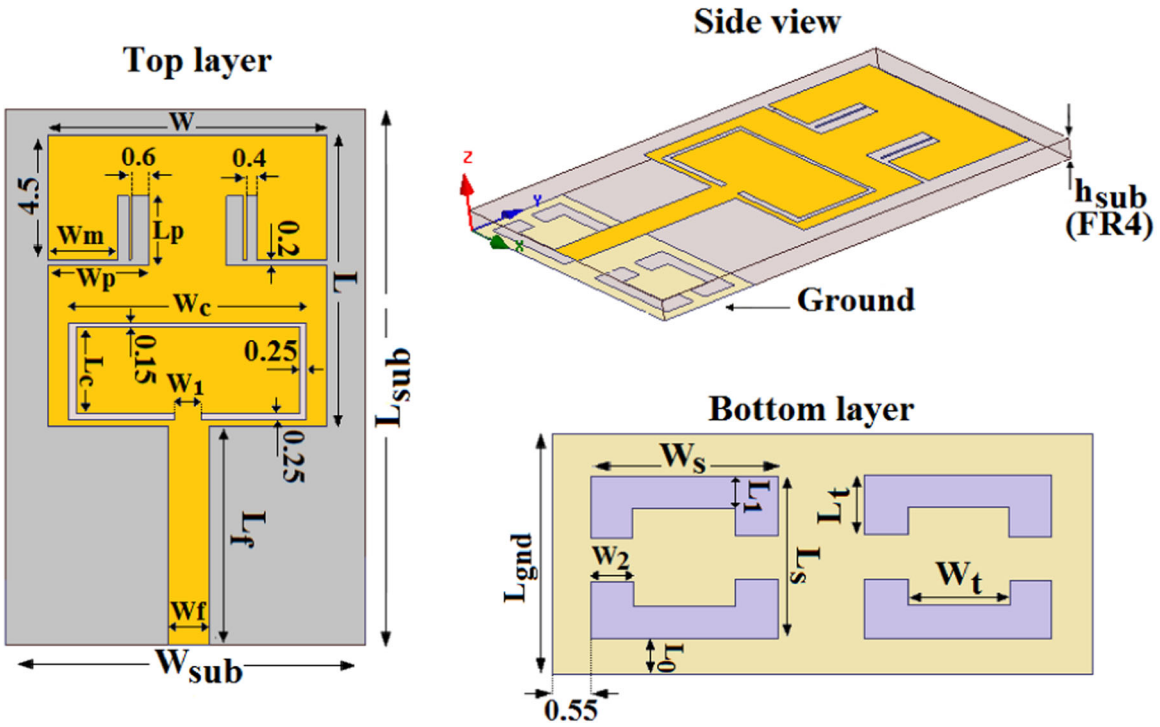

FIGURE 1 Configuration and parameters of the proposed printed monopole antenna (unit: mm).

TABLE 1 The best-fit parameters of the proposed antenna.

Parameter	mm	Parameter	mm	Parameter	mm
W_{sub}	12	L_{sub}	18	h_{sub}	0.8
W	10	L	10	W_f	1.5
L_f	7	L_{gnd}	4	W_c	8.5
L_c	3.1	W_1	1	W_p	3.6
W_m	2.6	L_p	2.5	W_S	4.5
W_t	2.5	L_t	1.3	L_1	0.5
W_2	0.93	L_0	0.5	L_S	3

decreases with a reduction in this factor. This is contingent upon the width of the radiating patch, along with the dielectric constant and thickness and of the proposed substrate. The best-fit parameters of the proposed antenna are specified in Table 1.

3 | RESULTS AND DISCUSSIONS

In this segment, we investigate different aspects of the designed printed monopole antenna, adjusting each parameter independently while maintaining the others constant. To achieve a thorough comprehension of the antenna's performance and ascertain ideal parameter settings, we conducted an analysis using HFSS software.

Figure 2A demonstrates the progressive stages of expanding our antenna, outlining the stepwise procedure employed for simulation studies focusing on multi-resonance and dual band-stop capabilities. The illustration portrays the creation of a novel antenna by integrating two sets of U-shaped slots into the ground plane. Incorporating these slots on both sides of the feedline amplifies the overall bandwidth. Figure 2B showcases the influence of dual sets of U-shaped slots with varying dimensions on impedance matching, contrasting them with the same antenna configuration but lacking slots. Analysis indicates that the conventional antenna, devoid of both bandwidth-enhancing features and filter structures, showcases wideband performance spanning from 3.1 to 10.6 GHz for voltage standing wave ratio (VSWR) < 2. Notably, the integration of the two pairs of U-shaped slots notably enhances the impedance bandwidth, particularly at the upper-frequency range. The specifics dimensions of three distinct cases for the presented antenna are as follows: Case1 ($W_S = 4$ mm, $L_S = 3.25$ mm, $W_t = 3$ mm, $L_t = 1.25$ mm, and $L_1 = 0.75$ mm), Case2 ($W_S = 4.75$ mm, $L_S = 3.5$ mm, $W_t = 3.5$ mm, $L_t = 1.5$ mm, and $L_1 = 0.4$ mm), and Case3 ($W_S = 4.5$ mm, $L_S = 3$ mm, $W_t = 2.5$ mm, $L_t = 1.3$ mm, and $L_1 = 0.5$ mm).

The specific arrangement of the two sets of U-shaped slots significantly widens the impedance bandwidth,

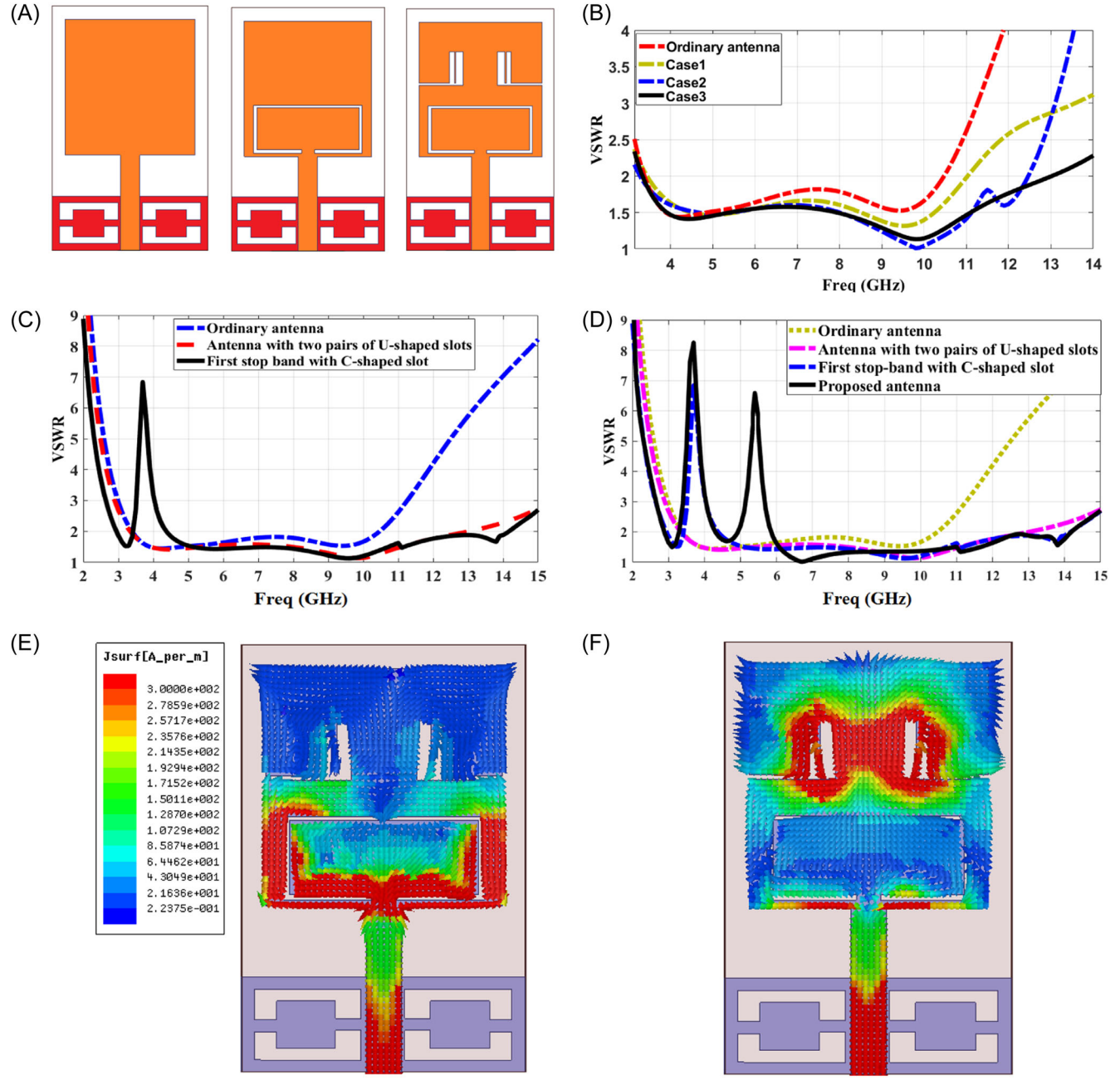

FIGURE 2 (A) The step-by-step development of the antenna used for multiresonance and band-stop performances, (B) the effects of the two pairs of U-shaped slots with different values, (C) simulated VSWR characteristics for the antennas shown in (A), (D) simulated VSWR characteristics for the whole antennas shown in (A), (E) simulated surface current distributions on radiating patch for the proposed antenna at 3.65 GHz, and (F) simulated surface current distributions on radiating patch for the proposed antenna at 5.6 GHz. VSWR, voltage standing wave ratio.

particularly in the higher frequency ranges. The enhancement in impedance matching across the entire frequency range is attributed to the implementation of DGS, which introduces supplementary surface current pathways within our antenna configuration. Furthermore, our ground-plane design featuring the DGS structure modifies the capacitive and inductive properties of the input impedance, resulting in changes to the impedance bandwidth.[3]

The following phase in advancing the proposed antenna design centers on establishing the length of the band-stop slots. This process, illustrated in Figure 2C, incorporating a modified C-shaped slot structure into the radiation patch is aimed at incorporating the characteristics of the initial band-stop within the C-band (3.7–4.2 GHz) and WiMAX (3.3–3.6 GHz). Additionally, the incorporation of this slot structure facilitates a notably expanded impedance bandwidth. Furthermore,

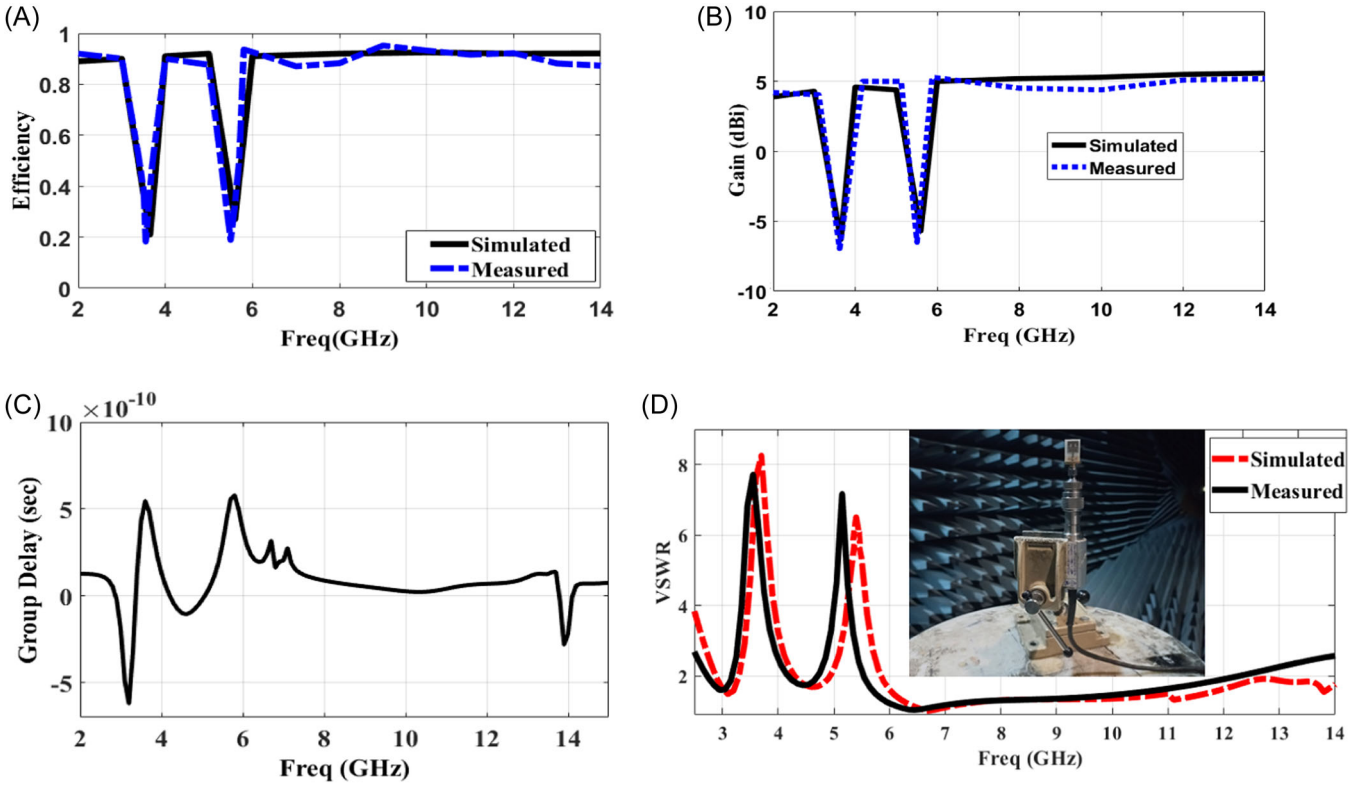

FIGURE 3 (A) The simulated and measured radiation efficiency of the optimized ultra-wideband (UWB) antenna with filter structures, (B) the simulated and measured maximum gain of the optimized UWB antenna with filter structures, (C) simulated group delay of the proposed antenna, and (D) photograph of the fabricated antenna and comparison between measured and simulated VSWR for the proposed antenna. VSWR, voltage standing wave ratio.

as illustrated in Figure 2D, to establish the second band-stop frequency within the WLAN (5.2/5.8-GHz) band, a pair of F-shaped slots is integrated into the radiation patch. Each slot functions as a resonator at its respective band-stop frequency.

The length of the resonant slot, which is a multiple of quarter-wavelength, can be approximately determined as $L_{\text{total}} \cong n\lambda_g/4$. To obtain the desired band-stop frequency, the wavelength is determined by $\lambda_g = \lambda/\sqrt{\varepsilon_{\text{reff}}}$, where λ denotes the free space wavelength and $\varepsilon_{\text{reff}}$ is the effective dielectric constant ($\varepsilon_{\text{reff}} \cong (\varepsilon_r + 1)/2$).[7] In our designed scheme, an effective starting point for the length (L_{stop1}) is set at 3.65 GHz, with a guided wavelength (λ_{gstop1}) of 50.02 mm. The equivalent stub length for the first stop-band frequency is determined as:

$$L_{\text{stop1}} = (2 \times L_c) + (2 \times W_c) + (2 \times 0.15) - W_1 = 22.5\text{mm}. \quad (2)$$

This length is approximately half of the corresponding guided wavelength ($\lambda_{\text{gstop1}}/2 = 25.01$ mm). The second stop-band length, L_{stop2}, is set at 5.6 GHz, with a guided wavelength (λ_{gstop2}) of 32.6 mm. Similarly, the equivalent length for the second stopband frequency can be calculated as:

$$L_{\text{stop2}} = W_p + (2 \times L_p) = 8.6\text{mm}. \quad (3)$$

This length is roughly a quarter of the corresponding guided wavelength ($\lambda_{\text{gstop2}}/4 = 8.15$ mm). The required lengths for each stopband are determined using Equations (2) and (3) and integrated into the antenna design. These lengths are then refined through optimization in HFSS software to improve performance.

To facilitate a thorough comprehension of the band-stop capability inherent in the proposed printed monopole antenna, simulated current distribution in the radiation patch surrounding the band-stop structures is depicted in Figure 2E,F. As illustrated, within these structures at the focal points of the band-stop frequencies (3.65 and 5.6 GHz), currents primarily flow around the band-stop structures, displaying opposing directions along the outer and inner edges. Therefore, the resulting radiation fields oppose each other, achieving the desired high attenuation near the stop-band frequencies.[6]

Figure 3A,B illustrates the radiation efficiency and maximum gain of the dual band-stop capabilities antenna, as measured and simulated across the operating frequency spectrum. The plot indicates that the implemented dual-band-stop antenna consistently achieves

high gain and radiation efficiency, except for two stopped frequencies at 3.65 and 5.6 GHz. Beyond these stop bands, the antenna's gain remains relatively stable (with variations below 1.5 dB), demonstrating consistent performance across the operational band. The radiation efficiency of the designed antenna exceeds 90% throughout the operational band, confirming its efficacy within the desired frequency ranges and exhibiting suitable gain and radiation efficiency. Turning to Figure 3C, the simulated group delay of the antenna systems is depicted. The antenna exhibits an almost flat response in the 2.9–14.2 GHz frequency band, with minimal variation in group delay, staying below 0.5 ns except in the stop bands.

To verify the proposed design, a prototype of the antenna with optimized dimensions was manufactured, as depicted in Figure 3D. This figure also illustrates the VSWR characteristics of the proposed antenna, both measured and simulated. Notably, the measured results closely align with those obtained through simulation. It's important to highlight that the designed antenna, incorporating filter structures, exhibits two stop-bands capabilities at 3.3–4.2 GHz and 5.15–5.85 GHz, effectively covering WiMAX (3.3–3.6 GHz), C-band (3.7–4.2 GHz), and WLAN (5.2–5.8 GHz). Additionally, the antenna exhibits broad frequency coverage, maintaining performance from 2.9 to 14.2 GHz for VSWR < 2, encompassing the entire UWB frequency band.

The measured results closely resemble the simulated results, indicating the accuracy and validity of both the design and simulation models. This high correlation can be attributed to careful design, accurate modeling, and precise manufacturing processes. Furthermore, it's crucial to acknowledge a potential disparity between the measured and simulated results, which could be influenced by various factors such as the thickness and dielectric constant of the antenna substrate, and the prototype fabricated antenna dimensions. To ensure precise VSWR for the fabricated antenna, meticulous attention must be devoted to both the manufacturing and measurement processes.

Figure 4A illustrates the measured and simulated radiation patterns of the dual band-stop capabilities antenna at frequencies of 3, 7, and 12 GHz in two principal planes: The E-plane (yz-plane) and the H-plane (xz-plane). It is evident that the proposed antenna demonstrates relatively consistent

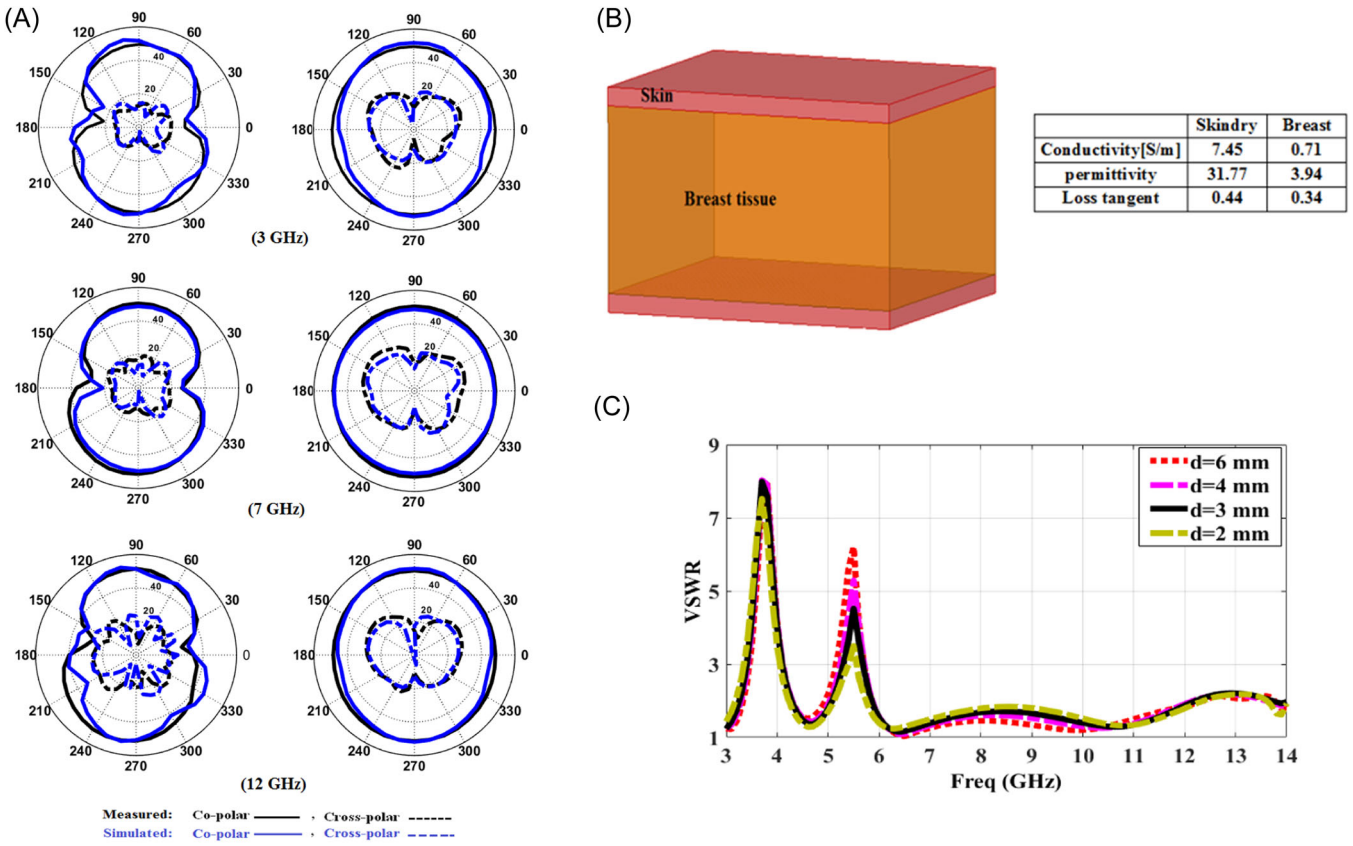

FIGURE 4 (A) Measured and simulated radiation patterns at frequencies 3, 7, and 12 GHz, (B) configuration of the compressed breast model with two antennas, (C) the VSWR of the proposed antenna in the vicinity of the phantom for different values of *d*, and (D) 10 g Specific Absorption Rate results at different frequencies for different values of *d*. VSWR, voltage standing wave ratio.

(D)

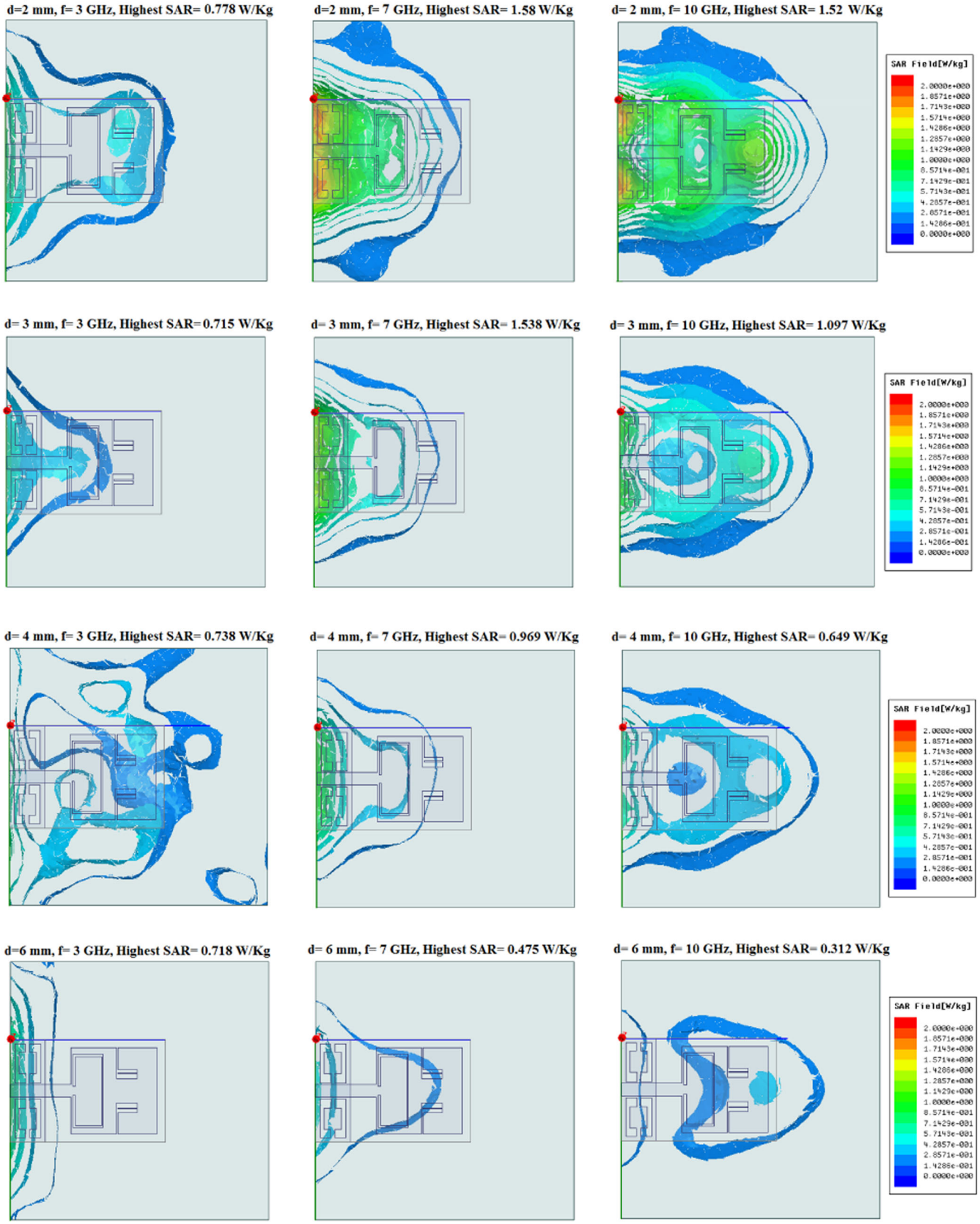

FIGURE 4 (Continued)

TABLE 2 Comparison of previous designs with the proposed antenna.

References	Bandwidth (GHz)	Peak gain (dBi)	Rejection bands (GHz)	Dimensions (mm^3)
[6]	2.8–11.8	4.8	3.3–3.8 5.1–6	$20 \times 18 \times 1$
[7]	3–11.2	5	3.3–3.85 5.05–5.9	$18 \times 14 \times 1$
[8]	2.96–15.8	6.1	Without rejection band	$18 \times 12 \times 0.8$
[14]	2.63–11.66	4	3.15–3.66 4.9–5.9	$30 \times 20 \times 1$
[15]	3.1–11	4.47	5–5.4 7.8–8.4	$32 \times 24 \times 0.76$
[16]	2.64–12.9	6.7	4.8–5.9 7.1–7.8	$31 \times 30.5 \times 1.575$
[17]	2.6–14	2.89	5.58–5.91 7.02–7.45	$36 \times 30 \times 0.762$
[18]	2.66–14.86	3.6	3.01–3.63 4.48–5.85	$35 \times 29 \times 0.762$
[19]	2.5–11	4.9	5.2–5.7 7.2–8.5	$32 \times 24 \times 1.6$
[20]	3.1–15.5	5.8	3.3–4.2 5–6	$20 \times 20 \times 0.8$
This work	2.9–14.2	5.1	3.3–4.2 5.2–5.8	$18 \times 12 \times 0.8$

omnidirectional radiation patterns in the xz-plane, while in the yz-plane, the radiation patterns adopt a dumbbell shape. Cross-polarization levels typically exhibit significantly lower levels compared to their co-polarization counterparts.

To evaluate the impact of the human body phantom on the band-stop frequencies of the proposed antenna, assessments were carried out in close proximity to a human body model. This model incorporates skin and breast tissues, as depicted in Figure 4B. The electromagnetic characteristics of these layers, such as relative permittivity, conductivity, and loss tangent at 9.5 GHz, are detailed in.[8] The dimensions of the human body model are $90 \times 90 \times 45$ mm, featuring a skin layer of identical size and a thickness of 2 mm positioned on the top and bottom.

Figure 4C illustrates the impact of varying distances between the antenna and the human body model on the antenna's matching. The parameter d signifies the separation between the antenna and the phantom. The findings reveal a reduction in the VSWR value in the second stop-band, while the stability of the first stop-band is sustained near the human body model. Moreover, a noticeable enhancement in the second stop-band is apparent with increasing d. Across other frequencies, the antenna's VSWR consistently remains below 2. These observations suggest that the proposed antenna demonstrates a broad bandwidth with dual band-stop characteristics in close proximity to the phantom.

The SAR is a measure used to evaluate the safety thresholds of in-body antennas, as elevated SAR values can adversely affect biological systems. SAR10g assessments are conducted, with international guidelines capping the SAR limit at 2 W/kg averaged over any 10 g of tissue. To analyze the antenna's impact on tissue, a basic skin tissue model was used. Considering the tissue's conductivity and permittivity properties (Figure 4B), the highest SAR results from the simulation are shown in Figure 4D. The maximum SAR level for the antenna is 1.58 W/kg, which complies is acceptable for both FCC and ICNIRP standards. As illustrated in Figure 4D, increasing the d value results in a decrease in the maximum SAR value.

Table 2 compares the proposed antenna with other recent designs. Given the large number of antennas featuring bandstop characteristics, only UWB antennas with dual bandstop capabilities are included in Table 2 to ensure a meaningful comparison. The table shows that the proposed antenna is notably compact, with a reduced footprint and increased impedance bandwidth relative to previously reported UWB antennas. Additionally, it exhibits reasonable peak gain values.

4 | CONCLUSIONS

A novel square monopole antenna has been introduced, distinguished by its compact design and featuring dual-band-stop characteristics alongside wide bandwidth suitable for UWB applications. The assessment of the designed antenna was conducted both in free space and in close proximity to a breast phantom. By integrating two pairs of U-shaped slots on the ground plane, which contributed to a broad usable fractional bandwidth exceeding 132%, the antenna achieved a wide impedance bandwidth. The incorporation of a C-shaped slot and a pair of F-shaped slots in the radiation patch generated dual stop bands suitable for WiMAX, C-band, and WLAN applications. The antenna's gain exhibited an almost flat response within the operational frequency band, with two sharp decreases observed in the stop bands. The

findings indicate that the antenna operates effectively within the desired frequency bands, demonstrating a radiation efficiency of over 90%. Finally, the study examining the effect of the human body model on the stop bands was presented, and the designed antenna demonstrated suitable performance for use in in-body microwave applications.

DATA AVAILABILITY STATEMENT

The data that support the findings of this study are available from the corresponding author upon reasonable request.

ORCID

Mousa Abdollahvand https://orcid.org/0000-0001-5579-423X

REFERENCES

1. Federal Communications Commission. *First Report and Order on Ultra-Wideband Technology*. 2002. Scientific Research.
2. Naser-Moghadasi M, Dadashzadeh GR, Abdollahvand M, Zehforoosh Y, Virdee BS. Planar triangular monopole antenna with multioctave bandwidth. *Microw Opt Technol Lett*. 2011;53:10-14.
3. Abdollahvand M, Dadashzadeh GR. Compact double-fed dual annular ring printed monopole antenna for UWB application. *J Electromagn Waves Appl*. 2009;23:1969-1980.
4. Abdollahvand M, Hassani HR, Dadashzadeh GR. Novel modified monopole antenna with band-notch characteristic for UWB application. *IEICE Electron. Express*. 2010;7:1207-1213.
5. Abdollahvand M, Dadashzadeh GR, Ebrahimian H, Ojaroudi M. Compact ultra-wideband printed monopole antenna having frequency band-notch characteristic using defected ground structure. *Microw Opt Technol Letts*. 2011;53:2363-2368.
6. Abdollahvand M, Dadashzadeh G, Mostafa D. Compact dual band-notched printed monopole antenna for UWB application. *IEEE Antennas Wirel Propag Lett*. 2010;9:1148-1151.
7. Abdollahvand M, Abbasi-Arand B, Katoch K, Ghosh S. A novel and compact ultra-wideband printed monopole antenna with enhanced bandwidth and dual-band stop properties. *Microw Opt Technol Lett*. 2024;66:e33990.
8. Abdollahvand A, Pirhadi A, Ebrahimian H, Abdollahvand M. A compact UWB printed antenna with bandwidth enhancement for in-body microwave imaging applications. *Prog Electromagn Res C*. 2014;55:149-157.
9. Dilruba Geyikoglu M. A novel UWB flexible antenna with dual notch bands for wearable biomedical devices. *Analog Integr Circuits Signal Process*. 2023;114:439-450.
10. Li X, Jalilvand M, Sit YL, Zwick T. A compact double-layer on-body matched bowtie antenna for medical diagnosis. *IEEE Trans Antennas Propag*. 2014;62:1808-1816.
11. El Atrash M, Abdalgalil OF, Mahmoud IS, Abdalla MA, Zahran ShR. Wearable high gain low SAR antenna loaded with backed all-textile EBG for WBAN applications. *IET Microw Antennas Propagation (Online)*. 2020;14:791-799.
12. Singh K, Dhayal M, Dwivedi S. Breast cancer detection by terahertz UWB microstrip patch antenna loaded with 6X6 SRR array. *IETE J Res*. 2023;5295-5310.
13. Mahmood SN, Ishak AJ, Ismail A, Soh AC, Zakaria Z, Alani S. On-Off body ultra-wideband (UWB) antenna for wireless body area networks (WBAN): a review. *IEEE Access*. 2020;8:150844-150863.
14. Çelik K. A novel circular fractal ring UWB monopole antenna with dual band-notched characteristics. *ETRI J*. 2023;46:1-9.
15. Yadav D, Abegaonkar MP, Koul SK, Tiwari V, Bhatnagar D. A compact dual band-notched UWB circular monopole antenna with parasitic resonators. *AEU-I J Electron Commun*. 2018;84:313-320.
16. Wang Y, Huang T, Ma D, Shen P, Hu J, Wu W. Ultra-wideband (UWB) monopole antenna with dual notched bands by combining electromagnetic-bandgap (EBG) and slot structures. *IEEE MTT-S Int Microw Biomed Conference (IMBioC)*. 2019. http://dx.doi.org/10.1109/IMBIOC.2019.8777856
17. Rai VK, Kumar M. Tunable inverted U-shaped dual band notch monopole antenna for ultrawideband applications. *IETE J Res*. 2021;69:1-11.
18. Grandhi Venkata S, Kalva SRK. UWB monopole antenna with dual notched bands verified by characteristic mode analysis (CMA). *Prog Electromagn Res C*. 2022;121:39-48.
19. Kumar OP, Ali T, Kumar P, Kumar P, Anguera J. An elliptical-shaped dual-band UWB notch antenna for wireless applications. *Appl Sci*. 2023;13:1310.
20. Ojaroudi Parchin N, Basherlou HJ, Abd-Alhameed RA. UWB microstrip-fed slot antenna with improved bandwidth and dual notched bands using protruded parasitic strips. *Prog Electromagn Res C*. 2020;101:261-273.

How to cite this article: Abdollahvand M, Zehforoosh Y, Marufi B, Kaleybar PE, Dastranj A. A novel UWB in-body printed microstrip feed monopole antenna with dual band-stop capabilities. *Microw Opt Technol Lett*. 2024;66:e34317. doi:10.1002/mop.34317